Analytica Chimica Acta 1070 (2019) 88–96

Contents lists available at ScienceDirect

Analytica Chimica Acta

journal homepage: www.elsevier.com/locate/aca

Rapid synthesis of Au/Ag bimetallic nanoclusters with highly biochemical stability and its applications for temperature and ratiometric pH sensing

Huanhuan Sun, Taiping Qing, Xiaoxiao He**, Jingfang Shangguan, Ruichen Jia, Hongchang Bu, Jin Huang, Kemin Wang*

State Key Laboratory of Chemo/Biosensing and Chemometrics, College of Biology, College of Chemistry and Chemical Engineering, Hunan University, Key Laboratory for Bio-Nanotechnology and Molecule Engineering of Hunan Province, Changsha, 410082, China

HIGHLIGHTS

- A simple and robust approach was developed for preparing Au/Ag NCs within dozens of minutes.
- This synthetic route endowed Au/Ag NCs with prominently enhanced biochemical stability.
- A sensitive fluorescent thermometer was handily fabricated based on an Au/Ag NCs-loaded straw.
- A ratiometric nanosensor was subtly designed and utilized for pH sensing based on the incorporation of FITC into the Au/Ag NCs.
- The high stable Au/Ag NCs hold the potential as a candidate for promoting the development of biomedical research field.

GRAPHICAL ABSTRACT

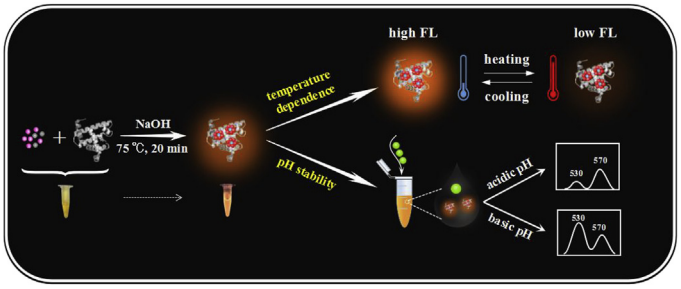

ARTICLE INFO

Article history:
Received 14 December 2018
Received in revised form
9 April 2019
Accepted 12 April 2019
Available online 16 April 2019

Keywords:
Bimetallic nanoclusters
Biochemical stability
Fluorescent thermometer
pH sensing
Ratiometric nanosensor
Silver/gold

ABSTRACT

Herein, we developed a simple and rapid strategy to synthesize gold/silver bimetallic nanoclusters (Au/Ag NCs) with highly biochemical stability by a one-pot route. The Au/Ag NCs were obtained via a chemical reduction procedure in alkaline aqueous solution at 75 °C within only 20 min by employing bovine serum albumin (BSA) as both ligand and reductant. The as-obtained Au/Ag NCs displayed bright orange fluorescence with an emission peak located at 570 nm and temperature-dependent fluorescence property, which were utilized as fluorescent thermometer directly. More intriguingly, the Au/Ag NCs were very stable against various pH values, ions, biothiols, H_2O_2, fetal bovine serum (FBS), RPMI 1640 medium and amino acids. Taking advantage of the excellent biochemical stability, a ratiometric fluorescence biosensor, fluorescein-5-isothiocyanate (FITC)-Au/Ag NCs, was constructed for pH sensing based on the incorporation of FITC into the Au/Ag NCs. Furthermore, the ratiometric pH sensor was also successfully applied on the model of HeLa cells.

* Corresponding author.
** Corresponding author.
E-mail addresses: xiaoxiaohe@hnu.edu.cn (X. He), kmwang@hnu.edu.cn (K. Wang).

https://doi.org/10.1016/j.aca.2019.04.029
0003-2670/

1. Introduction

Fluorescent metal nanoclusters (e.g., Au, Cu, Ag, Pt and Pd NCs) that consisting of several to hundreds of atoms have drawn substantial attention owing to their distinct properties of good biocompatibility, subnanometer size, large Stokes shift, narrow and tunable fluorescence spectrum [1–4]. These unique characteristics endowed them as desirable nanosensors for widespread applications in the area of environmental and biomedical science [5–10]. Strongly promoted by the development of these monometallic NCs, bimetallic NCs emerged as a kind of novel and promising nanomaterial, which integrating two metal species into one cluster [11–13]. Compare to monometallic NCs, 1) the physicochemical properties and electronic structures of two metal species could be integrated into one bimetallic nanoclusters [14,15], 2) more attractive advantages for optical, catalytic and electronic performance via controlling their compositions and sizes due to the synergistic effects [16,17]. On this account, unremitting efforts have been done on high-quality synthesis and promising applications of bimetallic NCs (e.g., Au/Pd, Au/Cu, Cu/Ag and Au/Ag NCs) over the past few years [11,12,18–24]. For example, it was demonstrated that the indraught of Au atoms to the surface of Pd NCs largely enhanced their catalytic activity towards glucose oxidation [18]. Au/Cu NCs have been fabricated and applied through the indraught of Cu to alter the fluorescent properties of Au NCs [13]. Remarkably, the bimetallic NCs of Au/Ag NCs have attained extensive attention due to their unique synergistic effects of obvious intrinsic fluorescence, high biocompatibility and ultrasmall sizes. For instance, Au/Ag NCs with enhanced luminescence were prepared by the doping of silver into Au NCs owing to the "silver effect" [19–22]. Tang's group synthesized highly fluorescence Au/Ag NCs and utilized for the sensing of pyrophosphatase activity [23]. Red-emitting Au/Ag NCs were obtained in Wang's group for the fluorescence imaging of Fe^{3+} in living cells thanks to their low cytotoxicity [24].

Up to now, a series of synthetic procedures have been explored for Au/Ag NCs, which could be classified into two types of co-reduction synthesis and post-treatment route [25–28]. In 2009, Chang et al. reported a method for the preparation of different sizes of Au/Ag nanoparticles by controlling the molar ratios of Ag ions to Au ions [29]. T. Pradeed group reported the synthesis of luminescent AuAg alloy nanoclusters in bovine serum albumin for the first time [30]. In this work, the Au/Ag NCs were obtained by mixing two kinds of metal nanoclusters or adding $HAuCl_4$ to Ag NCs. Although these approaches endowed the nanoclusters with strong fluorescence emissions covering blue to near infrared via picking kinds of templates and adjusting the concentration of reductant and templates/metal ions molar ratio, a time-consuming reaction process, tedious preparation procedure, poor water solubility, broad size distribution and/or expensive templates are still need to be resolved.

For another, the biochemical stability of fluorescent nanosensors is of crucial importance to their applications. Several factors, such as pH of the environment condition [31,32], the existence of homologous analytes and photobleaching in fluorescence [33], may cause the sensors to output false-positive signals, allowing us to make inaccurate qualitative or quantitative analysis and limiting their practical application under complex conditions. For the purpose of extending their applications to bioimaging with reliable performance, the creation of Au/Ag NCs that are equipped with enhanced biochemical stability for the real-time detection in biological environments when challenged with potential interferences and various conditions is also highly desirable.

With this in mind, we developed a simple and rapid approach to synthesize gold/silver bimetallic nanoclusters (Au/Ag NCs) with highly biochemical stability. As illustrated in Scheme 1, the Au/Ag NCs were obtained through BSA-mediated co-reduction of Au^{3+} and Ag^{+} at 75 °C within only 20 min by a one-pot strategy. The as-obtained Au/Ag NCs displayed bright orange fluorescence with an emission peak located at 570 nm and showed temperature-dependent fluorescent property and excellent biochemical stability. Taking advantage of these properties, a sensitive fluorescent thermometer was handily fabricated based on an Au/Ag NCs-loaded straw. In addition, a ratiometric fluorescence biosensor, consisting of pH-insensitive Au/Ag NCs as reference probe and pH-sensitive fluorescein-5-isothiocyanate (FITC) as report probe, was also developed for pH sensing. It was demonstrated that the constructed pH sensor exhibits good linear relationship against pH values in buffer solution and remarkable resolution for intracellular pH imaging on the example of HeLa cells.

2. Experiment

2.1. Chemicals and reagents

Bovine serum albumin (BSA) was obtained from Shanghai Sangon Biotechnology Co. Ltd. (China). NaOH, Hydrogen tetrachloroaurate tetrahydrate ($HAuCl_4 \cdot 4H_2O$, >99%), Silver nitrate ($AgNO_3$, 99%), mercury, copper and other metal salts were obtained from Sinopharm Chemical Reagent Co. Ltd. (Shanghai, China). Fluorescein 5(6)-isothiocyanate (FITC) was purchased from Aldrich

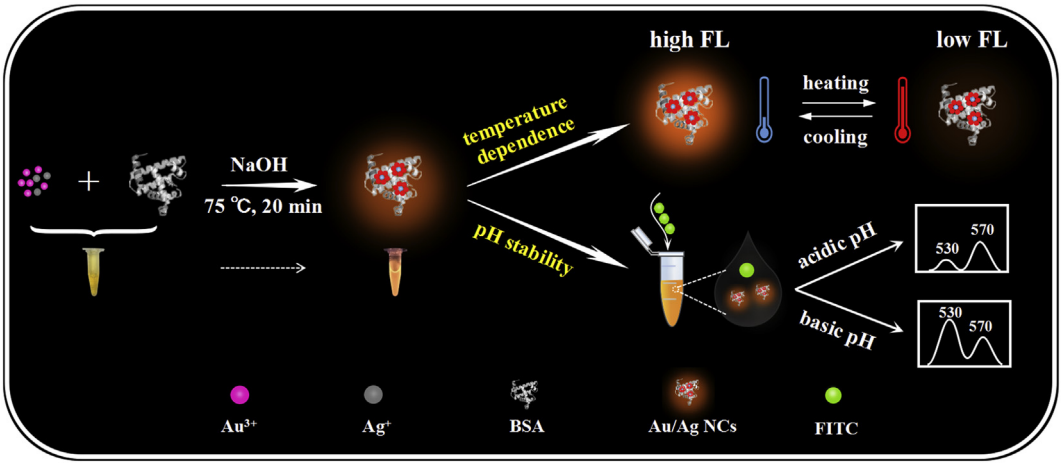

Scheme 1. Synthesis of BSA-Au/Ag NCs and its applications for temperature and pH sensing.

(St. Louis, MO, U.S.A.). 4,6-Diamidino-2-phenylindole (DAPI) was from Gen-view Scientific Inc. (U.S.A). The amino acid solutions were prepared freshly on the day of use. All solvents and chemicals are the analytical grade and used without further purification. Ultrapure Milli-Q water (18.2 MΩ cm-1, Milli-Q, Millipore) was used for all experiments.

2.2. Apparatus

All the measurements of fluorescence spectroscopy were measured using a Hitachi F-7000 fluorescence spectrophotometer (Tokyo, Japan) and the fluorescence images of cells were obtained on a Nikon A1 (Nikon, Japan). The photographs of corresponding reaction products were recorded on a WD-9403 UV Transilluminator (Beijing, China) at 365 nm. The high-resolution transmission electron microscopy (HRTEM) images were conducted on Tecnai G2 20 Swin (FEI, Czech Republic). X-ray photoelectron spectra (XPS) analyses were recorded with ESCALAB 250Xi spectrometer. All the pH measurements were acquired on a San-Xin MP511 miniature pH meter (Shanghai, China).

2.3. Preparation of BSA-Au/Ag NCs

Initially, the $HAuCl_4$ aqueous solution (100 μL, 100 mM) and $AgNO_3$ solution (50 μL) with different concentrations were added to 750 μL of BSA solution (66.7 mg mL^{-1}) under gentle stirring at room temperature for 2 min. The reaction conditions were optimized via a series of temperatures (35, 55, 65, 70, 75, 80 and 90 °C) and for various of durations (5, 10, 15, 20, 25 and 30 min). Then, NaOH (100 μL, 1 M) solution was introduced into the mixture and the reaction was to proceed under the optimal reaction condition. Finally, the as-synthesized Au/Ag NCs were purified by exhaustive dialysis against distilled water through a 1 KDa molecular weight cut-off for 48 h to remove the free ions. The cleaned products were then freeze dried and stored at 4 °C for further use. As control, the same synthesis and purification procedures were used to preparation of BSA-Au NCs, BSA-Ag NCs with alkaline BSA solutions containing only Au^{3+} or Ag^{+}, respectively. The Au^{3+} and Ag^{+} were also added to the as-obtained Ag NCs and Au NCs respectively and reacted under the same condition.

2.4. Biochemical stability investigation of BSA-Au/Ag NCs

To evaluate the biochemical stability of BSA-Au/Ag NCs, we investigated the effect of various pH, metal ions, anions, biothiols, H_2O_2, fetal bovine serum (FBS), RPMI 1640 medium and amino acids on the fluorescence intensity. At first, we measured the fluorescence of as-prepared Au/Ag NCs solutions in various pH values from pH 2.0–9.0. Then, 190 μL of solutions containing 10 mg ml^{-1} Au/Ag NCs dissolved in different pH values (pH 3.0, 7.0, 11.0) and incubated with 10 μL of 2 mM metal ions, including Na^{+}, K^{+}, Mg^{2+}, Ca^{2+}, Zn^{2+}, Co^{2+}, Cr^{3+}, Mn^{2+}, Pb^{2+}, Cd^{2+}, Cu^{2+}, Ti^{2+}, Hg^{2+}, Fe^{3+}, Al^{3+}, Cr^{3+}, Zr^{4+}, Ag^{+} were mixed thoroughly, respectively. Under an excitation wavelength at 480 nm, the fluorescence spectra were then measured after the mixture was proceeded for 10 min. Also, the effects of anions (F^{-}, HCO_3^{-}, Cl^{-}, $S_2O_8^{2-}$, CO_3^{2-}, $H_2PO_4^{-}$, I^{-}, Br^{-}, SO_3^{2-}, SO_4^{2-}, NO_3^{-}, HPO_4^{-}) on the Au/Ag NCs were investigated by a similar procedure. Next, the influences of 10 mM biothiols (GSH, Cys), 1 mM amino acids, 20% FBS, 20% RPMI 1640 were tested with 10 mg ml^{-1} Au/Ag NCs respectively. In addition, the effect of photoillumination on the fluorescence of as-obtained Au/Ag NCs was also explored. Finally, the fluorescence of Au/Ag NCs were kept at 4 °C and measured for a total of 5 times in 3 months.

2.5. Construction of nanosensors for temperature and pH sensing

For temperature sensing, Au/Ag NCs solution (100 μL, 50 mg mL^{-1}) was injected into a quartz cuvette, equilibrated for 5 min after setting the temperature at series of points from 10 to 50 °C with an interval of 5 °C. To further probe the reversibility of Au/Ag NCs, the fluorescence switching operations were repeated for six consecutive cycles by implementing multiple heating and cooling cycles between 10 and 50 °C. The sensor was constructed by simply injecting Au/Ag NCs into a transparent straw, one end of which was sealed. Subsequently, the full-loaded straw was put into a water-filled flask for temperature sensing of the water sample through real-time monitoring the fluorescence intensity of Au/Ag NCs under 365 nm ultraviolet light.

To obtain a ratiometric fluorescence pH sensor with a suitable fluorescence spectrum, Au/Ag NCs (400 μL, 50 mg ml^{-1}) and FITC (100 μL) were dissolved in PBS (10 mM, 500 μL) at pH 9.0 to achieve a balance of two fluorescence emission peaks by optimization the concentration of FITC. Next, the fluorescence of optimal system was tested in PBS with different pH values (PBS = 10 mM, pH 6.0, 6.5, 7.0, 7.5, 8.0 and 8.5, 1 mL). Then, the FITC-Au/Ag NCs fluorescent nanosensor used for ratiometric pH sensing was prepared. Additionally, in order to confirm the biocompatibility of FITC-Au/Ag NCs, MTT assay was used for quantitative testing of the cell viability.

2.6. Cell culture and fixation

HeLa cells (human cervical cancer cell line) were cultured in RPMI 1640 medium supplemented with 10% fetal bovine serum (FBS, heat inactivated), 100 U/mL penicillin and gentamicin solution at 37 °C with 5% wt/vol CO_2 in a humidified atmosphere. For the cell fixation, HeLa cells were seeded on 35-mm glass bottom dishes and maintained for 36 h. Afterwards, the medium in the dishes was removed and cells were washed twice with phosphate buffered saline (PBS, pH 7.40, Ca^{2+} and Mg^{2+} free). And the cleaned cells were fixed on the dishes with 4% paraformaldehyde (PFA) for 9 min at room temperature and finally washes four times by PBS (pH 6.0, 6.5, 7.0, 7.5, and 8.0).

2.7. Confocal fluorescence imaging

The cleaned cells in dishes were incubated with clear medium containing FITC-Au/Ag NCs for 3.5 h. Before imaging, the slides were stained with DAPI. Then, PBS with various pH values (pH 6.0, 6.5, 7.0, 7.5, and 8.0) were used to wash the cells for three times to remove excess probes and then added 100 μL PBS with corresponding pH values into dishes for 20 min to equilibrate the intracellular pH. The confocal fluorescent images of cells were performed with a 100 × oil immersion objective. Excitation wavelength and emission filters were set as follows: Ex = 405 nm, Em = 425–475 nm (DAPI); Ex = 488 nm, Em = 500–550 nm (FITC); Ex = 488 nm, Em = 570 nm-620 nm (Au/Ag NCs).

3. Results and discussions

3.1. Synthesis of BSA-Au/Ag NCs

In this work, chemical reduction method was used to synthesize the fluorescent BSA-Au/Ag NCs in the presence of $HAuCl_4$ and $AgNO_3$ as metal precursors by employing BSA as ligand and reductant. Firstly, the effect of silver doping on the fluorescence spectrum of BSA-Au NCs was explored, as demonstrated in Fig. S1, the fluorescence spectrum of BSA-Au NCs displayed a 630 nm emission upon 500 nm excitation (line a), which was consistent with previous reports [34]. Then, the fluorescence of the product

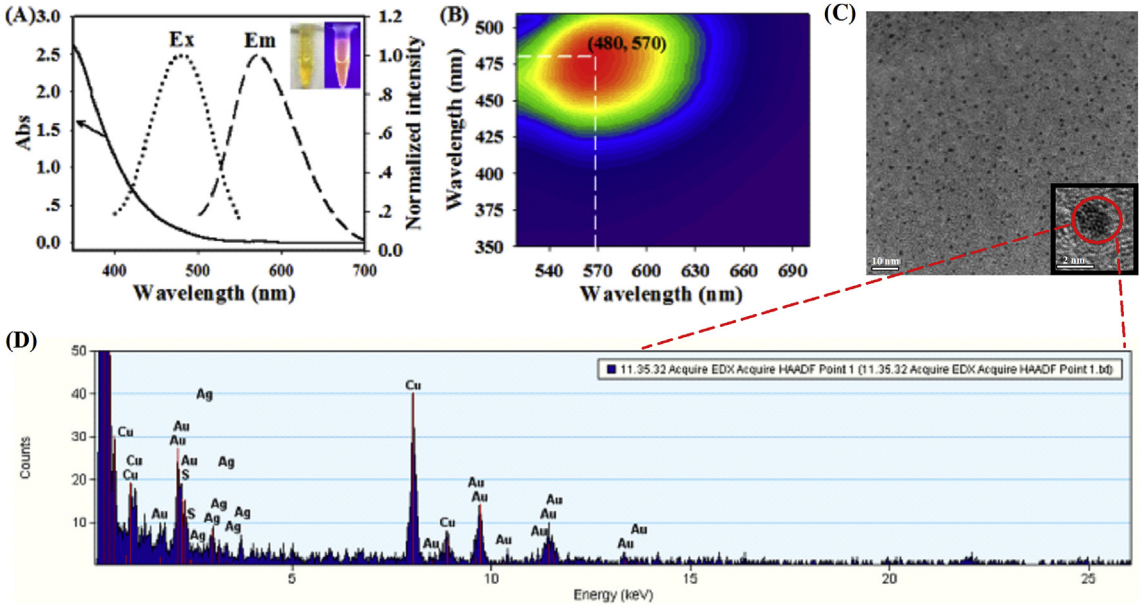

Fig. 1. (A) UV–Vis absorption spectra and fluorescence spectroscopy of Au/Ag NCs. Insert: photographs under sun light (left) and UV light (right). (B) 3D scan of Au/Ag NCs. (C) HRTEM image (D) EDS of Au/Ag NCs.

with only $AgNO_3$ as metal precursor was so weak that could be considered negligible (line b). However, the emission peak at 570 nm with distinct orange fluorescence could be observed from the synthesized product using $HAuCl_4$ and $AgNO_3$ as co-reaction precursors (line c). Additionally, the fluorescence spectra of the mixture containing as-synthesized Au NCs and silver ions (line d), Au NCs and Ag NCs (line e), Ag NCs and gold ions (line f), were also measured. The concentrations of gold and silver ions were the same as the above reactions and the mixtures were incubated for long enough time. It was found that the fluorescence intensity of the line e and the line f were weak or absent, while that of the line d was decreased by more than half with a blue-shift of emission peak to 600 nm, which have been reported in previous works [35]. Given the above, the characterization of fluorescence spectra preliminarily demonstrated that the BSA-Au/Ag NCs was successfully synthesized by one-pot strategy.

To obtain the BSA-Au/Ag NCs with highest possible fluorescence emission intensity, the basic reaction conditions of temperature, reaction time and molar ratio (Au^{3+}/Ag^{+}) were optimized orderly. Firstly, the reaction temperature was optimized, as depicted in

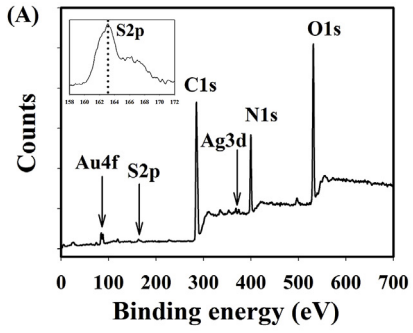

(B)

Element	Atomic %
C 1s	61.78
O 1s	21.11
N 1s	16.03
Au 4f	0.28
Ag 3d	0.15

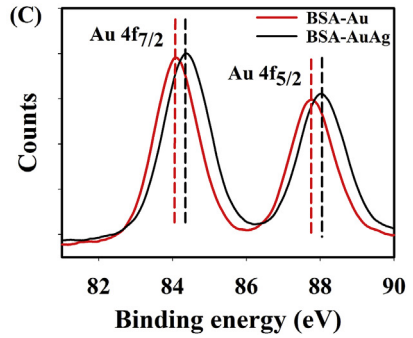

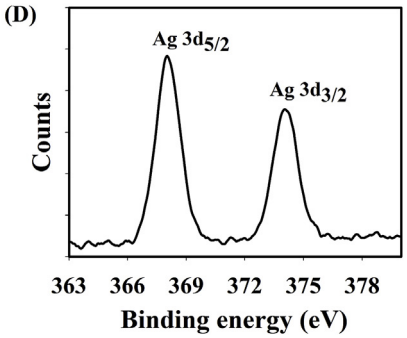

Fig. 2. (A) XPS survey spectrum of Au/Ag NCs showing the presence of metallic Ag and Au. (B) The atomic percentage of the main elements of Au/Ag NCs. (C) XPS spectra of Au 4f for Au/Ag NCs and Au NCs. (D) XPS spectrum of Ag 3d for Au/Ag NCs.

Fig. S2, the result showed a red shift of emission peak and a trend of increasing firstly and then decreasing in fluorescence intensity as the temperature rose up. Then, the effect of reaction time was investigated. It was displayed that the trend of fluorescence intensity change was the same as the temperature variation while the emission wavelength only increased to 570 nm at maximum (Fig. S3). Finally, we explored the effect of molar ratio (Au^{3+}/Ag^{+}) on the fluorescence (Fig. S4). The result revealed that the increased concentration of silver ions always be with a continuously blue shift of emission peak and decrease of intensity. Based on the above results, we decided to use the molar ratio (Au^{3+}/Ag^{+}) of 10:5 setting at 75 °C for 20 min to prepare Au/Ag NCs with stable and highly fluorescence for further investigation.

3.2. Characterization

The optical, morphological and structural properties of the as-prepared Au/Ag NCs were characterized. It was observed that Au/Ag NCs suspension exhibited yellow color under daylight and bright orange color under 365 nm ultraviolet light (Fig. 1A, insert). The UV–vis spectrum revealed that the Au/Ag NCs had a broad absorption band under 480 nm. Additionally, the excitation and emission fluorescence spectra were highly symmetrical with a maximum peak centered at 480 nm and 570 nm, respectively (Fig. 1A). As we can see in Figure 1B, 3D-scan of Au/Ag NCs was exactly consistent with the result. The quantum yield (QY) of the Au/Ag NCs was measured using Rhodamine 6G as a standard (measured at 570 nm excitation wavelength, QY = 95% in ethanol). The average quantum yield (QY) of Au/Ag NCs in aqueous solution at room temperature was about 3.4%. The morphological images of the Au/Ag NCs were characterized by high-resolution transmission electron microscopy (HRTEM). As illustrated in Fig. 1C, the Au/Ag NCs show high monodispersity. The average particle diameter of the Au/Ag NCs was 1.28 nm. There was no obvious core-shell structure or lattice mismatch observed for Au/Ag NCs (Fig. 1C, insert), indicating that they probably be formed in bimetallic alloys.

For further confirmation, the structure of the Au/Ag NCs was investigated by means of energy dispersive spectroscopy (EDS) and X-ray photoelectron spectroscopy (XPS). As depicted in Fig. 1D, the EDS results confirmed that the Au/Ag NCs were composed of gold and silver elements. Besides, the main elements and atomic percentages of the Au/Ag NCs were recorded by XPS (Fig. 2A and B). Compare to Au NCs, Au/Ag NCs had higher binding energy values of 88.04 eV for Au $4f_{5/2}$ and 84.39 eV for Au $4f_{7/2}$, which suggested that the Au electrons of Au/Ag NCs were bound more tightly because of the introduction of Ag atoms (Fig. 2C and D) [36,37]. Besides, the presence of S 2p (163.03eV) was assigned to Au/Ag-S binding while the absence of typical oxidized sulfur (at about 168.0 eV) indicated a favorable chemical stability of the Au/Ag NCs (Fig. 2A, insert) [38]. Both of EDS and XPS analysis have further proved the successful preparation of the Au/Ag NCs. We next investigated the optical properties of the as-obtained Au/Ag NCs.

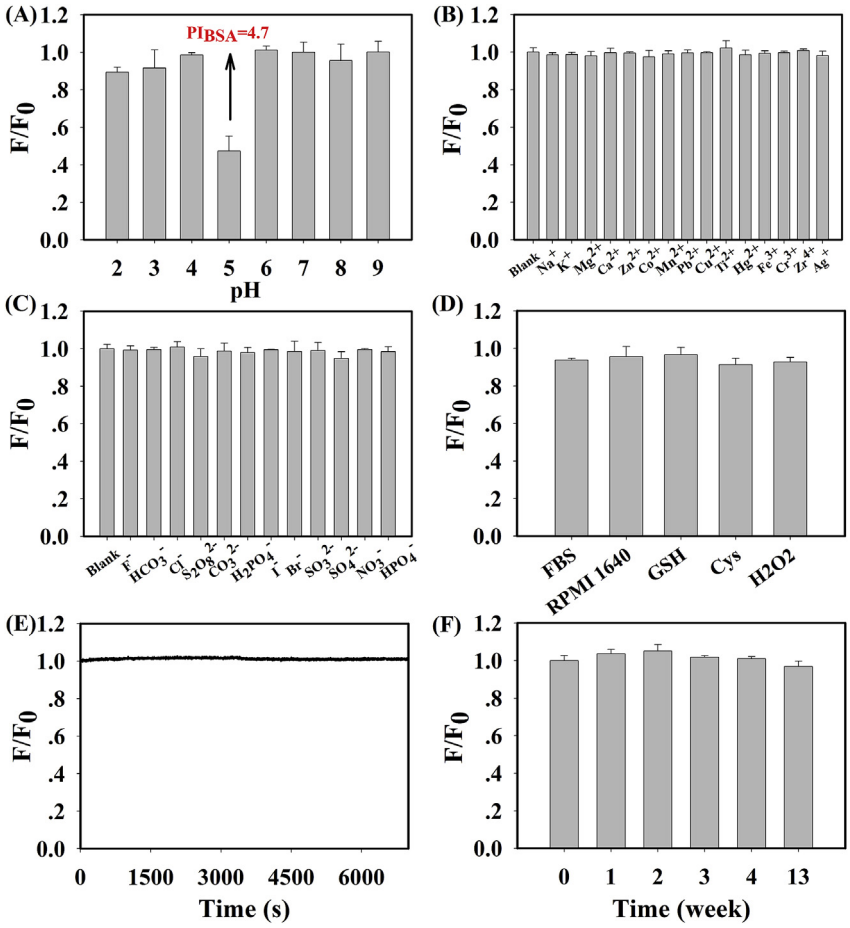

Fig. 3. Effects of (A) pH values (B) common metal ions in 100 μM (C) common anions in 100 μM (D) 20% FBS, 20% RPMI 1640 medium, biothiols in 10 mM and H_2O_2 in 100 mM (E) fluorescent timescan for 2 h (D) storage time on the fluorescence intensity of BSA-Au/Ag NCs.

3.3. Biochemical stability of BSA-Au/Ag NCs

For the purpose of verifying whether the Au/Ag NCs have the essential stability and anti-interference ability for bearing circumstance as an optical sensor, we examined the effect of pH, ions, biothiols, FBS and other potential interferences on their fluorescence properties. As depicted in Fig. 3A, the Au/Ag NCs exhibited good solubility and stability in the pH range of 2.0–9.0 except the pH value of 5, where was approximate to the isoelectric point of BSA (PI = 4.7) and led to the appearance of precipitates and a decrease of fluorescence intensity. Furthermore, the fluorescent stability of Au/Ag NCs toward potential interferences, including various common metal ions, anions, biothiols, H_2O_2, FBS and RPMI 1640 were generally explored. As illustrated in Fig. 3B, C, 3D, there was no marked change on the fluorescence intensity in the presence of potential interferences under neutral condition. The effects of these potential interferences on Au/Ag NCs under alkaline and acidic condition were then tested (Fig. S5). Moreover, the effects of other amino acids were also investigated carefully (Fig. S6). The data demonstrated the good fluorescence stability of the Au/Ag NCs. Additionally, there was no obvious fluorescent change and precipitate of Au/Ag NCs after a fluorescent time scan for 2 h of excitation at 480 nm and being stored in darkness at 4 °C at least for 3 months (Fig. 3E and F). These results revealed the excellent biochemical stability and fluorescent stability of Au/Ag NCs, enabling them as promising candidate for practical applications.

3.4. Fluorescent response of BSA-Au/Ag NCs toward temperature

To explore the potential application of the Au/Ag NCs as a fluorescent thermometer, the fluorescence spectra in a temperature range of 10–50 °C were recorded. Intriguingly, the fluorescent intensity of Au/Ag NCs exhibited dramatically temperature-dependent property. As shown in Fig. 4A, the emission intensity decreased regularly with temperature rose from 10 to 50 °C. Nevertheless, the emission wavelengths always kept constant with the variation of temperature, suggesting the high purity of as-prepared Au/Ag NCs. By contrast, the fluorescence band of the quantum dots gradually red shifted as the environmental temperature increased [39]. The fluorescence of Au/Ag NCs decreased

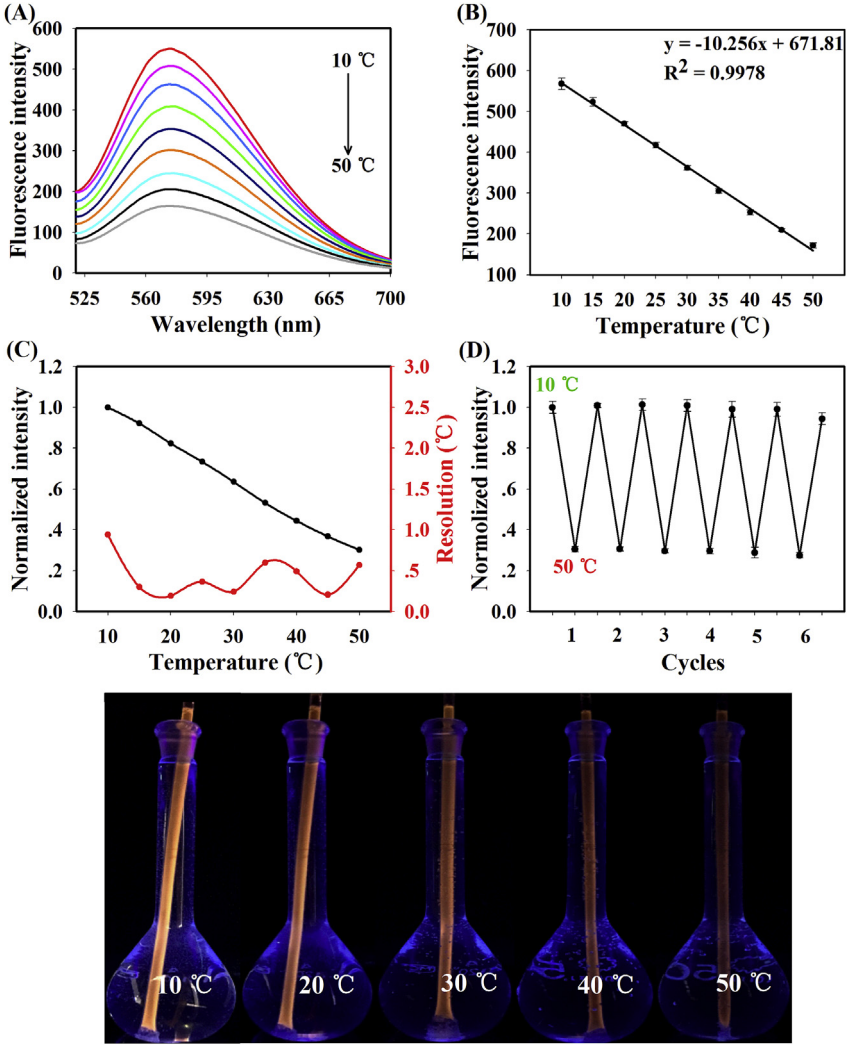

Fig. 4. (A) Temperature-dependent fluorescence spectra of Au/Ag NCs (50 mg·mL-^{1}) in the range of 10–50 °C. (B) The corresponding linear calibration curve at 570 nm. (C) Black dotted line is the normalized fluorescence curve of the Au/Ag NCs, as a function of temperature. The fluorescence emissions were collected under the laser excitation at 480 nm. Red dotted line is relative temperature resolution. (D) The fluorescence response of Au/Ag NCs upon cycling between 10 °C and 50 °C for six consecutive cycles. (E) Digital photos of the Au/Ag NCs solution as a fluorescent thermometer for temperature sensing at 10 °C, 20 °C, 30 °C, 40 °C, 50 °C under UV light. (For interpretation of the references to color in this figure legend, the reader is referred to the Web version of this article.)

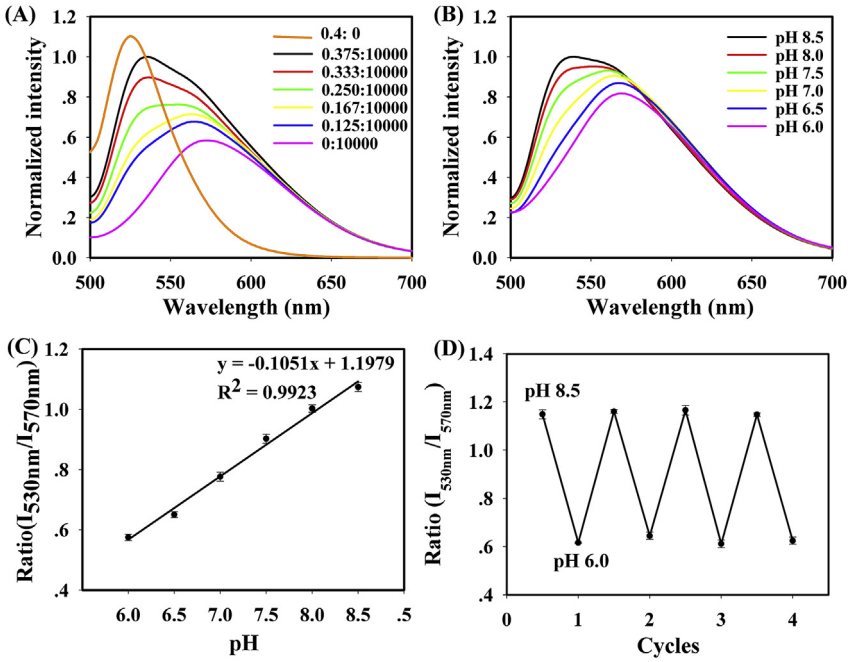

Fig. 5. (A) Fluorescence spectra of FITC-Au/Ag NCs measured at different mass ratio of FITC: NCs with pH 9.0. (B) Fluorescence spectrum of FITC-Au/Ag NCs in PBS buffer with different pH values range from 6.0 to 8.5 under 480 nm excitation wavelength. (C) Linear relationship of the ratiometric fluorescence intensity ($I_{530\ nm}/I_{570\ nm}$) versus pH values. (D) Fluorescence reversibility against pH change between 6.0 and 8.5, repeatedly.

linearly ($R^2 = 0.9978$) with the temperature rose from 10 to 50 °C (Fig. 4B). The temperature resolution of the fluorescent thermometer can be calculated by an equation, $\delta T = \frac{\partial T}{\partial FI}\delta FI$ [40], where $\frac{\partial T}{\partial FI}$ and δFI represent the inverse slope in the fluorescence intensity-temperature graph and the standard deviation of the average fluorescence intensity, separately. It was calculated that the temperature resolutions of Au/Ag NCs between 15 and 50 were 0.1–0.5 °C (Fig. 4C). As a reference, a whole comparison with other fluorescent thermometry system was introduced in Table S1 [41], which clearly confirmed the Au/Ag NCs was comparable to or better than the resolution of current fluorescent thermometer. Furthermore, the reversible process of resultant Au/Ag NCs between 10 and 50 °C were repeated for six consecutive cycles. As illustrated in Fig. 4D, the Au/Ag NCs present a good reproducibility between the wide temperature differences. On the basis of preliminary results, we concluded that the Au/Ag NCs showed a good performance in fluorescence stability and temperature resolution, which have the potential to be developed as a fluorescent nanosensor for precise temperature sensing.

To explore the practical application of as-prepared Au/Ag NCs as a temperature sensor, we injected them into a transparent straw sealed at the bottom to monitor the temperature variations of the water sample. As shown in Fig. 4E, a bright orange fluorescence of Au/Ag NCs could be observed at low temperature under 365 nm ultraviolet light, upon elevating the temperature of water increasingly, the fluorescence intensity of the full-loaded straw declined gradually. The results indicated that the BSA-Au/Ag NCs could function as a fluorescent probe to construct a nanosensor for temperature sensing.

3.5. pH sensing with FITC-Au/Ag NCs

With the development of synthetic strategies of metal nanoclusters, the mono/bimetallic nanoclusters have been involved in exciting advances of analytical methods for fluorescent biosensing and bioimaging [25,42]. For example, Tseng group developed a nanosensor based on FITC-conjugated protein gold nanoclusters for ratiometric pH sensing [43]. Considering the excellent biochemical stability and fluorescent stability of the as-obtained Au/Ag NCs, we reasoned that a ratiometric sensor could also be developed for pH sensing based on the mixture containing FITC as a measure probe and Au/Ag NCs as an internal standard, respectively. The pH-sensitive behavior of the FITC doped Au/Ag NCs were examined in 10 mM PBS buffer with different pHs. The fluorescence spectra of FITC-Au/Ag NCs with a series of mass ratio of FITC to Au/Ag NCs were investigated first. As depicted in Fig. 5A, FITC-Au/Ag NCs displayed two distinct emission peaks of FITC and Au/Ag NCs with a mass ratio of 0.333:10000 at pH = 9.0, which was selected as the fluorescent probe for pH sensing (Fig. 5B). The fluorescence intensity ratios ($I_{530\ nm}/I_{570\ nm}$) of this sensing system had a linear relationship ($R^2 = 0.9923$) in the range of pH 6.0–8.5 (Fig. 5C). Moreover, two different pH values at both ends were set to explore the fluorescence reversibility of this system (Fig. 5D). The result showed that the fluorescent ratio ($I_{530\ nm}/I_{570\ nm}$) between pH 6.0–8.5 floated up and down within a constant range over several cycles. In addition, no obvious cytotoxicity was observed when HeLa cells were incubated with FITC-Au/Ag NCs (Fig. S7). As a consequence, the FITC-Au/Ag NCs as a pH sensor was equipped with prominent advantages, such as easy to synthesis, anti-interference ability, pH-dependent fluorescent ratio, and great reusability.

3.6. Bioimaging application

The excellent biochemical stability and reversibility in the physiological pH range inspired us to further explore bioimaging application of the FITC-Au/Ag NCs in cancer cell system. As shown in Fig. 6A, the fluorescence intensity of FITC (green pseudocolor) in cells was gradually enhanced while that of the Au/Ag NCs (red pseudocolor) was slightly changed. With the pH value increasing from 6.0 to 8.0, the fluorescence of Au/Ag NCs channel kept generally unchanged while the FITC channel get brighter gradually, leading to an apparent color change of the merge graphs. Then, the

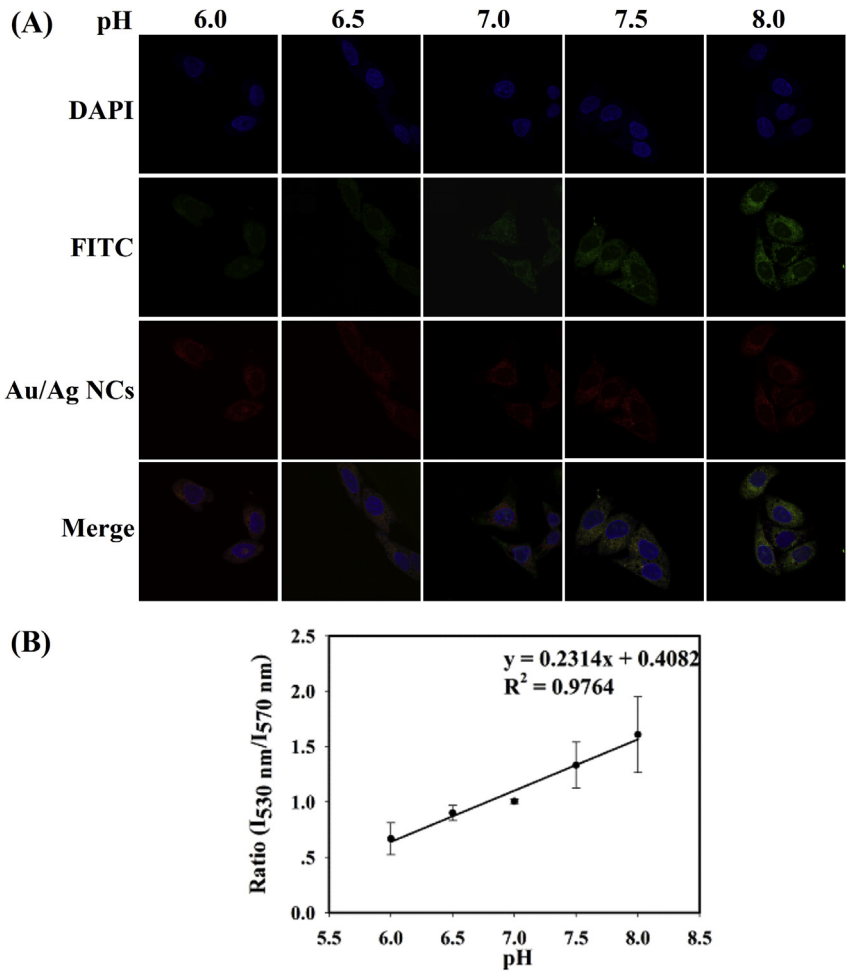

Fig. 6. (A) Confocal fluorescence images of FITC-Au/Ag NCs incubating with fixed HeLa cells at different pH. The blue fluorescence represents DAPI stained cell nuclei, the green fluorescence represents FITC, and the red fluorescence represents Au/Ag NCs. The merge image represents an overlay of the DAPI, FITC, and Au/Ag NCs signals. (B) Calibration curve of intracellular pH sensing. (For interpretation of the references to color in this figure legend, the reader is referred to the Web version of this article.)

average fluorescence intensity of the Au/Ag NCs and FITC under different pHs was computed respectively using ImageJ software. As depicted in Fig. 6B, the linear relationship between the fluorescence intensity ratio (I_{green}/I_{red}) and the pH values was attained range from 6.0 to 8.0 on the model of HeLa cancer cell.

4. Conclusion

In summary, we have described a simple and rapid approach for fabricating a highly stable Au/Ag NCs within dozens of minutes by employing BSA as both ligand and reductant. The as-obtained Au/Ag NCs exhibit obvious orange fluorescence and temperature-dependent property, which were utilized as fluorescent thermometer. The fluorescence intensity of Au/Ag NCs is linear against temperature ranging from 10 to 50 °C with reversibility and favorable resolution as high as 0.1–0.5 °C. What's more impressive is that, the Au/Ag NCs are demonstrated highly biochemical stability toward various pH values, ions, biothiols, H_2O_2, fetal bovine serum (FBS), RPMI 1640, amino acids and photoillumination. Due to the outstanding advantages, a ratiometric biosensor was designed for pH sensing by incorporating pH sensitive FITC dyes into Au/Ag NCs. The fluorescence intensity ratio($I_{530\ nm}/I_{570\ nm}$) of FITC-Au/Ag NCs also have a satisfactory linear relationship with the pH values in the range of 6.0–8.5 in buffer solution and good resolution for intracellular pH sensing in HeLa cells. Therefore, with ingenious design on the strength of the highly stable BSA-Au/Ag NCs, we anticipate that it can be employed as a candidate for biolabeling and bioimaging, which holds the potential for promoting the development of biomedical research field.

Declaration of interests

The authors declare that they have no known competing financial interests or personal relationships that could have appeared to influence the work reported in this paper.

The authors declare the following financial interests/personal relationships which may be considered as potential competing interests.

Acknowledgment

This work was supported by the Project of Natural Science Foundation of China (Grants 21675046, 21735002, 21521063 and 21874035). The key point research and invention program of Hunan province (2017DK2011).

Appendix A. Supplementary data

Supplementary data to this article can be found online at https://doi.org/10.1016/j.aca.2019.04.029.

References

[1] Y.Z. Lu, W. Chen, Sub-nanometre sized metal clusters: from synthetic challenges to the unique property discoveries, Chem. Soc. Rev. 41 (2012) 3594–3623.

[2] B. Adhikari, A. Banerjee, Facile synthesis of water-soluble fluorescent silver nanoclusters and HgII sensing, Chem. Mater. 22 (2010) 4364–4371.

[3] H. Kawasaki, K. Hamaguchi, I. Osaka, R. Arakawa, pH-Dependent synthesis of pepsin-mediated gold nanoclusters with blue green and red fluorescent emission, Adv. Funct. Mater. 21 (2011) 3508–3515.

[4] T.P. Qing, X.X. He, D.G. He, X.S. Ye, J.F. Shangguan, J.Q. Liu, B.Y. Yuan, K.M. Wang, Dumbbell DNA-templated CuNPs as a nano-fluorescent probe for detection of enzymes involved in ligase-mediated DNA repair, Biosens. Bioelectron. 94 (2017) 456–463.

[5] F. Liu, T. Bing, D.H. Shangguan, M. Zhao, N. Shao, Ratiometric fluorescent biosensing of hydrogen peroxide and hydroxyl radical in living cells with lysozyme–silver nanoclusters: lysozyme as stabilizing ligand and fuorescence signal Unit, Anal. Chem. 88 (2016) 10631–10638.

[6] L. Zhang, Q.Y. Cai, J. Li, G. Jia, J.Y. Wang, Z.Z. Dong, Z.H. Li, A label-free method for detecting biothiols based on poly (thymine)-templated copper nanoparticles, Biosens. Bioelectron. 69 (2015) 77–82.

[7] C. Dai, C.X. Yang, X. Yan, Self-quenched gold nanoclusters for turn-on fluorescence imaging of intracellular glutathione, Nano Res 11 (2018) 2488–2497.

[8] Z.Z. Dong, L. Zhang, M. Qiao, G. Jia, A.L. Liu, Z.H. Li, A label-free assay for T4 polynucleotide kinase/phosphatase activity and its inhibitors based on poly (thymine)-templated copper nanoparticles, Talanta 146 (2016) 253–258.

[9] Y.F. Lei, L.X. Tang, Y.Z.Y. Xie, Y.L. Xianyu, L.M. Zhang, P. Wang, Y. Hamada, K. Jiang, W.F. Zheng, X.Y. Jiang, Gold nanoclusters-assisted delivery of NGF siRNA for effective treatment of pancreatic cancer, Nat. Commun. 8 (2017) 15130.

[10] S.S. Zhou, L. Zhang, Q.Y. Cai, Z.Z. Dong, X. Geng, G. Jia, Z.H. Li, A facile label-free aptasensor for detecting ATP based on fluorescence enhancement of poly (thymine)-templated copper nanoparticles, Anal. Bioanal. Chem. 408 (2016) 6711–6717.

[11] J.K. Ahn, H.Y. Kim, S. Baek, H.G. Park, A new s-adenosylhomocysteine hydrolase-linked method for adenosine detection based on DNA-templated fluorescent Cu/Ag nanoclusters, Biosens. Bioelectron. 93 (2017) 330–334.

[12] R.C. Jin, K. Nobusada, Doping and alloying in atomically precise gold nanoparticles, Nano Res 7 (2014) 285–300.

[13] P.C. Chen, J.Y. Ma, L.Y. Chen, G.L. Lin, C.C. Shih, T.Y. Lin, H.T. Chang, Photoluminescent AuCu bimetallic nanoclusters as pH sensors and catalysts, Nanoscale 6 (2014) 3503–3507.

[14] C. Kumara, A. Dass, AuAg alloy nanomolecules with 38 metal atoms, Nanoscale 4 (2012) 4084–4086.

[15] D. Wang, Y. Li, Bimetallic nanocrystals: liquid-phase synthesis and catalytic applications, Adv. Mater. 23 (2011) 1044–1060.

[16] Q.B. Zhang, J.P. Xie, J.L. Liang, J.Y. Lee, Synthesis of monodisperse ag-au alloy nanoparticles with independently tunable morphology, composition, size, and surface chemistry and their 3-D superlattices, Adv. Funct. Mater. 19 (2009) 1387–1398.

[17] J. Yang, E.H. Sargent, S.O. Kelley, J.Y. Ying, A general phase-transfer protocol for metal ions and its application in nanocrystal synthesis, Nat. Mater. 8 (2009) 683–689.

[18] H.J. Zhang, T. Watanabe, M. Okumura, M. Haruta, N. Toshima, Catalytically highly active top gold atom on palladium nanocluster, Nat. Mater. 11 (2011) 49–52.

[19] N. Zhang, Y.M. Si, Z.Z. Sun, L.J. Chen, R. Li, Y.C. Qiao, H. Wang, Rapid, selective, and ultrasensitive fluorimetric analysis of mercury and copper levels in blood using bimetallic gold-silver nanoclusters with “silver effect”-enhanced red fluorescence, Anal. Chem. 86 (2014) 11714–11721.

[20] Q.F. Zhai, H.H. Xing, X.W. Zhang, J. Li, E.K. Wang, Enhanced electrochemiluminescence behavior of Au-Ag bimetallic nanoclusters and its sensing application for Hg(II), Anal. Chem. 89 (2017) 7788–7794.

[21] Q.F. Zhai, H.H. Xing, D.Q. Fan, X.W. Zhang, J. Li, E.K. Wang, Gold-Silver bimetallic nanoclusters with enhanced fluorescence for highly selective and sensitive detection of glutathione, Sens. Actuators, B 273 (2018) 1827–1832.

[22] Z.H. Li, R.Y. Liu, G.F. Xing, T. Wang, S.Y. Liu, A novel fluorometric and colorimetric sensor for iodide determination using DNA-templated gold/silver nanoclusters, Biosens. Bioelectron. 96 (2017) 44–48.

[23] Q. Zhou, Y. Lin, M. Xu, Facile synthesis of enhanced fluorescent gold-silver bimetallic nanocluster and its application for highly sensitive detection of inorganic pyrophosphatase activity, Anal. Chem. 88 (2016) 8886–8892.

[24] H. Huang, H. Li, J.J. Feng, A.J. Wang, One-step green synthesis of fluorescent bimetallic Au/Ag nanoclusters for temperature sensing and in vitro detection of Fe^{3+}, Sens. Actuators, B 223 (2016) 550–556.

[25] X. Yuan, X.Y. Dou, K.Y. Zheng, J.P. Xie, Recent advances in the synthesis and applications of ultrasmall bimetallic nanoclusters, Part, Sci. Technol. 32 (2015) 613–629.

[26] X.Y. Dou, X. Yuan, Y. Yu, Z.H. Luo, Q.F. Yao, D.T. Leong, J.P. Xie, Lighting up thiolated Au@Ag nanoclusters via aggregation-induced emission, Nanoscale 6 (2014) 157–161.

[27] T. Udayabhaskararao, Y. Sun, N. Goswami, S.K. Pal, K. Balasubramanian, T. Pradeep, Ag_7Au_6: a 13-atom alloy quantum cluster, Angew. Chem. Int. Ed. 51 (2012) 2155–2159.

[28] S.X. Wang, X.M. Meng, A. Das, T. Li, Y.B. Song, T.T. Cao, X.Y. Zhu, M.Z. Zhu, R.C. Jin, A 200-fold quantum yield boost in the photoluminescence of silver-doped Ag_xAu_{25-x} nanoclusters: the 13 th silver atom matters, Angew. Chem. Int. Ed. 53 (2014) 2376–2380.

[29] C.C. Huang, H.Y. Liao, Y.C. Shiang, Z.H. Lin, Z.S. Yang, H.T. Chang, Synthesis of wavelength-tunable luminescent gold and gold/silver nanodots, J. Mater. Chem. 19 (2009) 755–759.

[30] J.S. Mohanty, P.L. Xavier, K. Chaudhari, M.S. Bootharaju, N. Goswami, S.K. Pal, T. Pradeep, Luminescent bimetallic AuAg alloy quantum clusters in protein templates, Nanoscale 4 (2012) 4255–4262.

[31] H. Ao, Z.S. Qian, Y.Y. Zhu, M.Z. Zhao, C. Tang, Y.Y. Huang, H. Feng, A. Wang, A fluorometric biosensor based on functional Au/Ag nanoclusters for real-time monitoring of tyrosinase activity, Biosens. Bioelectron. 86 (2016) 542–547.

[32] H.Y. Xiong, W. Wang, J.C. Liang, W. Wen, X.H. Zhang, S.F. Wang, A convenient purification method for metal nanoclusters based on pH-induced aggregation and cyclic regeneration and its applications in fluorescent pH sensors, Sens. Actuators, B 239 (2017) 988–992.

[33] J. Zhang, Y. Yuan, F. Sun, G. Liang, Z. Jiang, S. Yu, Microwave-assisted synthesis of photoluminescent glutathione-capped Au/Ag nanoclusters: a unique sensor-on-a nanoparticle for metal ions, anions, and small molecules, Nano Res 8 (2015) 2329–2330.

[34] J.P. Xie, Y.G. Zheng, J.Y. Ying, Protein-directed synthesis of highly fluorescent gold nanoclusters, J. Am. Chem. Soc. 131 (2009) 888–889.

[35] Y. Yue, T.Y. Liu, H.W. Li, Z.Y. Liu, Y.Q. Wu, Microwave-assisted synthesis of BSA-protected small gold nanoclusters and their fluorescence-enhanced sensing of silver(I) ions, Nanoscale 4 (2012) 2251–2254.

[36] J. Sun, H.X. Wu, Y.D. Jin, Synthesis of thiolated Ag/Au bimetallic nanoclusters exhibiting an anti-galvanic reduction mechanism and composition-dependent fluorescence, Nanoscale 6 (2014) 5449–5457.

[37] R.J. Gui, H. Jin, Aqueous synthesis of human serum albumin-stabilized fluorescent Au/Ag core/shell nanocrystals for highly sensitive and selective sensing of copper (II), Analyst 138 (2013) 7197–7205.

[38] K. Kummer, D.V. Vyalikh, G. Gavrila, A. Kade, M. Weigel-Jech, M. Mertig, S.L. Molodtsov, High-resolution photoelectron spectroscopy of self-assembled mercaptohexanol monolayers on gold surfaces, J. Electron. Spectrosc. Relat. Phenom. 163 (2008) 59–64.

[39] L.L. Wang, J. Qiao, H.H. Liu, J. Hao, L. Qi, X.P. Zhou, D. Li, Z.X. Nie, L.Q. Mao, Ratiometric fluorescent probe based on gold nanoclusters and alizarin red-boronic acid for monitoring glucose in brain microdialysate, Anal. Chem. 86 (2014) 9758–9764.

[40] C. Gota, K. Okabe, T. Funatsu, Y. Harada, S. Uchiyama, Hydrophilic fluorescent nanogel thermometer for intracellular thermometry, J. Am. Chem. Soc. 131 (2009) 2766–2767.

[41] N.L. Xie, J. Huang, X.H. Yang, X.X. He, J.B. Liu, H.M. Fang, K.M. Wang, Scallop-Inspired DNA nanomachine: a ratiometric nanothermometer for intracellular temperature sensing, Anal. Chem. 89 (2017) 12115–12122.

[42] X.R. Song, N. Goswami, H.H. Yang, J.P. Xie, Functionalization of metal nanoclusters for biomedical applications, Analyst 141 (2016) 3126–3140.

[43] C.Y. Ke, Y.T. Wu, W.L. Tseng, Fluorescein-5-isothiocyanate-conjugated protein-directed synthesis of gold nanoclusters for fluorescent ratiometric sensing of an enzyme–substrate system, Biosens. Bioelectron. 69 (2015) 46–53.